

Dear Author,

Here are the proofs of your article.

- You can submit your corrections **online**, via **e-mail** or by **fax**.
- For **online** submission please insert your corrections in the online correction form. Always indicate the line number to which the correction refers.
- You can also insert your corrections in the proof PDF and **email** the annotated PDF.
- For fax submission, please ensure that your corrections are clearly legible. Use a fine black pen and write the correction in the margin, not too close to the edge of the page.
- Remember to note the **journal title**, **article number**, and **your name** when sending your response via e-mail or fax.
- **Check** the metadata sheet to make sure that the header information, especially author names and the corresponding affiliations are correctly shown.
- **Check** the questions that may have arisen during copy editing and insert your answers/ corrections.
- **Check** that the text is complete and that all figures, tables and their legends are included. Also check the accuracy of special characters, equations, and electronic supplementary material if applicable. If necessary refer to the *Edited manuscript*.
- The publication of inaccurate data such as dosages and units can have serious consequences. Please take particular care that all such details are correct.
- Please **do not** make changes that involve only matters of style. We have generally introduced forms that follow the journal's style. Substantial changes in content, e.g., new results, corrected values, title and authorship are not allowed without the approval of the responsible editor. In such a case, please contact the Editorial Office and return his/her consent together with the proof.
- If we do not receive your corrections **within 48 hours**, we will send you a reminder.
- Your article will be published **Online First** approximately one week after receipt of your corrected proofs. This is the **official first publication** citable with the DOI. **Further changes are, therefore, not possible.**
- The **printed version** will follow in a forthcoming issue.

#### **Please note**

After online publication, subscribers (personal/institutional) to this journal will have access to the complete article via the DOI using the URL: [http://dx.doi.org/\[DOI\]](http://dx.doi.org/[DOI]).

If you would like to know when your article has been published online, take advantage of our free alert service. For registration and further information go to: <http://www.link.springer.com>.

Due to the electronic nature of the procedure, the manuscript and the original figures will only be returned to you on special request. When you return your corrections, please inform us if you would like to have these documents returned.

# Metadata of the article that will be visualized in OnlineFirst

---

**Please note: Images will appear in color online but will be printed in black and white.**

---

ArticleTitle	Correlation Between Microstructure and Mechanical Properties Before and After Reversion of Metastable Austenitic Stainless Steels	
Article Sub-Title		
Article CopyRight	The Minerals, Metals & Materials Society and ASM International (This will be the copyright line in the final PDF)	
Journal Name	Metallurgical and Materials Transactions A	
Corresponding Author	Family Name	<b>Fargas</b>
	Particle	
	Given Name	<b>Gemma</b>
	Suffix	
	Division	CIEFMA - Departament de Ciència dels Materials i Enginyeria Metallúrgica
	Organization	Universitat Politècnica de Catalunya (CIEFMA-UPC)
	Address	Avda. Diagonal 647, 08028, Barcelona, Spain
	Email	<a href="mailto:gemma.fargas@upc.edu">gemma.fargas@upc.edu</a>
Author	Family Name	<b>Zapata</b>
	Particle	
	Given Name	<b>Ana</b>
	Suffix	
	Division	CIEFMA - Departament de Ciència dels Materials i Enginyeria Metallúrgica
	Organization	Universitat Politècnica de Catalunya (CIEFMA-UPC)
	Address	Avda. Diagonal 647, 08028, Barcelona, Spain
	Email	
Author	Family Name	<b>Roa</b>
	Particle	
	Given Name	<b>Joan Josep</b>
	Suffix	
	Division	CIEFMA - Departament de Ciència dels Materials i Enginyeria Metallúrgica
	Organization	Universitat Politècnica de Catalunya (CIEFMA-UPC)
	Address	Avda. Diagonal 647, 08028, Barcelona, Spain
	Email	
Author	Family Name	<b>Sapezanskaia</b>
	Particle	
	Given Name	<b>Ina</b>
	Suffix	
	Division	CIEFMA - Departament de Ciència dels Materials i Enginyeria Metallúrgica
	Organization	Universitat Politècnica de Catalunya (CIEFMA-UPC)
	Address	Avda. Diagonal 647, 08028, Barcelona, Spain
	Email	
Author	Family Name	<b>Mateo</b>

Particle	
Given Name	<b>Antonio</b>
Suffix	
Division	CIEFMA - Departament de Ciència dels Materials i Enginyeria Metallúrgica
Organization	Universitat Politècnica de Catalunya (CIEFMA-UPC)
Address	Avda. Diagonal 647, 08028, Barcelona, Spain
Email	

---

Schedule	Received
	Revised
	Accepted

---

Abstract	Reversion treatments are a way to improve the mechanical response of metastable austenitic stainless steels by means of grain refinement. To effectively apply those treatments, the steel must be previously deformed to induce a significant amount of martensitic transformation. In this work, the effect of reversion treatments was studied on a commercial AISI 301LN grade subjected to an industrial cold rolling process, with thickness reductions not higher than 40 pct. Microstructural changes and evolution of both monotonic and cyclic mechanical properties were investigated after cold rolling and upon reversion treatments. Results revealed that the finer austenitic microstructure obtained after reversion leads to an interesting combination of properties, with strong increments in hardness and yield strength, and also fatigue limit improvement, as compared to the initial annealed condition.
----------	--

---

Footnote Information	Manuscript submitted on December 11, 2014.
----------------------	--

---

Journal: 11661  
Article: 3178



## Author Query Form

**Please ensure you fill out your response to the queries raised below  
and return this form along with your corrections**

Dear Author

During the process of typesetting your article, the following queries have arisen. Please check your typeset proof carefully against the queries listed below and mark the necessary changes either directly on the proof/online grid or in the ‘Author’s response’ area provided below

<b>Query</b>	<b>Details required</b>	<b>Author’s response</b>
Figure 10	As per the information provided by the publisher, Fig. 10 will be black and white in print; hence, please confirm whether we can add “colour figure online” to the caption.	
General	Please check the edits made throughout the article and amend as required.	

# Correlation Between Microstructure and Mechanical Properties Before and After Reversion of Metastable Austenitic Stainless Steels



GEMMA FARGAS, ANA ZAPATA, JOAN JOSEP ROA, INA SAPEZANSKAIA,  
and ANTONIO MATEO

Reversion treatments are a way to improve the mechanical response of metastable austenitic stainless steels by means of grain refinement. To effectively apply those treatments, the steel must be previously deformed to induce a significant amount of martensitic transformation. In this work, the effect of reversion treatments was studied on a commercial AISI 301LN grade subjected to an industrial cold rolling process, with thickness reductions not higher than 40 pct. Microstructural changes and evolution of both monotonic and cyclic mechanical properties were investigated after cold rolling and upon reversion treatments. Results revealed that the finer austenitic microstructure obtained after reversion leads to an interesting combination of properties, with strong increments in hardness and yield strength, and also fatigue limit improvement, as compared to the initial annealed condition.

DOI: 10.1007/s11661-015-3178-8

© The Minerals, Metals & Materials Society and ASM International 2015

## I. INTRODUCTION

IN the past years, the demand for lightweight vehicles in order to reduce fuel consumption and also contaminant emissions has created interest in new materials to replace the classical carbon steel grades.<sup>[1]</sup> Austenitic stainless steels are presented as potential candidates for structural parts due to their excellent formability, weldability, and work hardening properties together with high corrosion resistance and high energy absorption capabilities. The main drawback is their relative low yield strength. It is well known that the addition of nitrogen is a way to improve mechanical properties by solid-solution strengthening.<sup>[2,3]</sup> Nevertheless, there is a limit for nitrogen solubility and problems with hot ductility may also appear. Strengthening by grain refining from dynamic recrystallization is another strengthening path, but severe deformations and high recrystallization temperatures are required.<sup>[4]</sup>

Among the austenitic stainless steels, those with thermodynamically metastable austenite at room temperature can be strengthening by grain refining applying thermo-mechanical processes. The procedure involves cold deformation of austenite to form strain-induced martensite followed by short annealing to revert the martensite into austenite. The amount of martensite

created depends on processing parameters such as temperature and deformation rate,<sup>[5]</sup> as well as on the steel composition.<sup>[6,7]</sup> Numerous investigations have shown that ultrafine and even nanograined austenite microstructures obtained from heavy cold rolling shows an excellent combination of mechanical strength and ductility<sup>[8-10]</sup> and also excellent fatigue strength<sup>[11]</sup> together with a higher corrosion resistance as compared with cold-rolled steel.<sup>[12]</sup>

AISI 301LN austenitic stainless steel is one of the commonly used stainless steel grades for light vehicles due to its excellent combination of formability and corrosion resistance. Thanks to its capability to transform to martensite under deformation; earlier studies have demonstrated that grain refinement up to ultrafine-grained austenite is feasible by means of reversion treatments. Those studies applied severe cold rolling deformation (45 to 77 pct of thickness reduction) to achieve final improvements in strength, ductility, and fatigue behavior.<sup>[13-16]</sup> On the other hand, a recent work carried on by Huang *et al.*<sup>[17]</sup> studied the effect of annealing temperature and time on the grain size of reversed austenite from 5 to 70 pct of strain-induced martensite obtained by advanced thermo-mechanical process, where cold rolling proceeds at 273 K (0 °C). Nevertheless, some authors<sup>[18,19]</sup> have noticed that the large amount of plastic deformation necessary for grain refinement requires special procedures to be efficient and that the resulting microstructure presents large variation in morphology which causes significant scatter in mechanical properties. In this sense, the present work is focused on conventional industrial process concerning the effect of cold rolling with a thickness reduction not higher than 40 pct range where no observations or data have been published to the authors' knowledge. Correlation between microstructure and mechanical

GEMMA FARGAS, Associate Professor, ANA ZAPATA and INA SAPEZANSKAIA Ph.D. Students, JOAN JOSEP ROA, Postdoctoral Researcher, and ANTONIO MATEO, Professor, are with the CIEFMA - Departament de Ciència dels Materials i Enginyeria Metallúrgica. Universitat Politècnica de Catalunya (CIEFMA-UPC). Avda. Diagonal 647, 08028, Barcelona, Spain. Contact e-mail: gemma.fargas@upc.edu

Manuscript submitted on December 11, 2014.



84 properties before and after reversion has been per- 140  
 85 formed regarding 10, 20, and 40 pct cold-rolled samples. 141  
 86 Microstructural evolution was analyzed by field emis- 142  
 87 sion scanning electron microscopy (FESEM) and elec- 143  
 88 tron back-scattered diffraction (EBSD) and mechanical 144  
 89 properties evaluated by tensile testing, hardness, and 145  
 90 also high-cycle fatigue (HCF) tests. 146

## 91 II. EXPERIMENTAL PROCESS

92 The experimental material was a commercial AISI 301 147  
 93 LN austenitic stainless steel (corresponding to standard 148  
 94 EN 1.4318) provided by OCAS NV, Arcelor-Mittal 149  
 95 R&D Industry Gent (Belgium). The chemical composi- 150  
 96 tion achieved by UV-Vis spectroscopy on a sample of 151  
 97 the studied steel randomly selected was (in wt pct): 152  
 98 Fe-0.03C-17.36Cr-7.18Ni-1.68Mn-0.23Mo-0.55Si-0.14N. 153  
 99 Sheets of 1.5 mm in thickness were supplied in four 154  
 100 different conditions: the steel named AR was subjected 155  
 101 to cold rolling, annealing, and pickling. The cold rolling 156  
 102 was carried out following 12 passes to achieve a 157  
 103 thickness reduction of 75 pct. Then, the steel was 158  
 104 annealed at 1323 K to 1353 K (1050 °C to 1080 °C) 159  
 105 for 10 minutes to recrystallize the deformed microstruc- 160  
 106 ture. All oxide scales were removed by passing the strip 161  
 107 through several consecutively mixed acid pickling baths, 162  
 108 and then finished off with high pressure water rinsing. 163  
 109 The three other conditions had an additional last cold 164  
 110 rolling step performed to achieve different percentages 165  
 111 of martensite. The thickness reductions were 10, 20, and 166  
 112 40 pct, for S1, S2, and S3 conditions, respectively. 167

113 Considering previous results,<sup>[20]</sup> the annealing for the 168  
 114 complete reversion to austenite microstructure was 169  
 115 carried out at 1023 K (750 °C) for 10 minutes. Samples 170  
 116 subjected to this treatment are called RS1, RS2, and 171  
 117 RS3, respectively. 172

118 Microstructural characterization was performed on 173  
 119 the rolling plane. For optical microscopy observations, 174  
 120 an Olympus LEXT light optical microscope was used 175  
 121 with confocal laser scanning mode. Samples were 176  
 122 ground and polished up to 1 μm and then electro-pol- 177  
 123 ished with 65 pct nitric acid solution at 12 V in order to 178  
 124 remove martensitic transformation induced during sur- 179  
 125 face preparation. Electro-etching at 1.5 V with the same 180  
 126 solution revealed austenitic grains. 15 images of each 181  
 127 studied steel condition were randomly selected and 182  
 128 characterized by image analysis in order to determine 183  
 129 the average grain size. 184

130 The phase components were identified by X-ray 185  
 131 diffraction with Copper radiation on a Bruker D8 186  
 132 Advance equipment. Determination of martensite con- 187  
 133 tent was carried out by the method corresponding to 188  
 134 reference intensity ratio (RIR), according to ASTM 189  
 135 E975-03.<sup>[21]</sup> This method allows determining the mass 190  
 136 fractions of austenite and martensite using Eq. [1]

$$\frac{X_{\alpha'}}{X_{\gamma}} = \frac{RIR_{\gamma}}{RIR_{\alpha'}} \times \frac{I_{\alpha', \text{observed}}}{I_{\gamma, \text{observed}}} \times \frac{I_{\gamma, \text{reference}}}{I_{\alpha', \text{reference}}}, \quad [1]$$

138 where  $X_{\alpha'}$  and  $X_{\gamma}$  are the mass fractions of  $\alpha'$ -martensite 191  
 139 and  $\gamma$ -austenite, respectively;  $RIR_{\gamma}$  and  $RIR_{\alpha'}$  are their 192

193 respective RIRs;  $I_{\text{observed}}$  and  $I_{\text{reference}}$  are the observed 194  
 195 and the reference intensities.<sup>[21]</sup> 196

197 EBSD scans were performed in a JSM-7001F FESEM 198  
 199 equipped with Channel 5 system (HKL Technology), 199  
 200 operating at 20 kV with samples tilted at 70 degrees. 200  
 201 EBSD measurements were performed at 50 nm of 201  
 202 scanning steps with beam currents of 9 nA. 202

203 Vickers hardness was measured with a MKV-HO de 203  
 204 Akashi tester using a 0.1 kg load. Ten indents were 204  
 205 carried out for each steel condition in order to determine 205  
 206 the average hardness value. Nanoindentation tests were 206  
 207 performed by a MTS Nanoindenter XP instrument 207  
 208 equipped with continuous stiffness measurement mod- 208  
 209 ulus. The characterization was performed with a 209  
 210 Berkovich tip indenter and the mechanical integrity, in 210  
 211 terms of hardness and elastic modulus, was analyzed 211  
 212 using the Oliver and Pharr method.<sup>[22,23]</sup> The indenter 212  
 213 shape was carefully calibrated with a fused silica 213  
 214 standard sample. Tests were carried out at a constant 214  
 215 deformation rate of  $5 \times 10^{-2} \text{ s}^{-1}$ . The mechanical 215  
 216 response for each specimen was assessed as the average 216  
 217 behavior of 25 indentations, organized in a regularly 217  
 218 spaced 5 by 5 array, at 500 nm penetration depth. A 218  
 219 constant distance between each imprint of 50 μm was 219  
 220 kept in order to avoid any overlapping effect. 220

221 Tensile testing was carried out at room temperature 221  
 222 using an INSTRON 8562 computerized universal testing 222  
 223 machine according to ASTM E 8-04,<sup>[24]</sup> at a strain rate 223  
 224 of  $4 \times 10^{-3} \text{ s}^{-1}$ . Yield strength ( $\sigma_{0.2}$ ), ultimate tensile 224  
 225 strength ( $\sigma_{\text{UTS}}$ ), and ductility were measured for all 225  
 226 studied steel conditions with samples were machine 226  
 227 aligned to rolling direction. Regarding ductility, percent 227  
 228 elongation (A pct) was computed considering the max- 228  
 229 imum elongation of the gage length divided by the 229  
 230 original gage length (25 mm). In order to determine the 230  
 231 amount of martensite formed during tensile tests, 231  
 232 interrupted tests were performed at 30, 60, and 90 pct 232  
 233 of the total elongation, and samples were extracted for 233  
 234 X-ray diffraction determination. 234

235 Considering the tensile properties, a fatigue testing 235  
 236 procedure was stated. It consisted of starting the tests by 236  
 237 applying a maximum load ( $\sigma_{\text{max}}$ ) of 50 pct of the 237  
 238 ultimate tensile strength of the corresponding steel 238  
 239 condition and afterwards, if the specimen was able to 239  
 240 reach  $10^6$  cycles without fail,  $\sigma_{\text{max}}$  was increased 10 pct, 240  
 241 and so on until fracture, following a staircase 241  
 242 method.<sup>[25]</sup> The value of the fatigue limit was determined 242  
 243 using the method proposed by Grove and Campan.<sup>[26]</sup> 243

244 Flat fatigue samples with hour-glass shape (Figure 1) 244  
 245 were laser machined from the steel sheets. As in the case 245

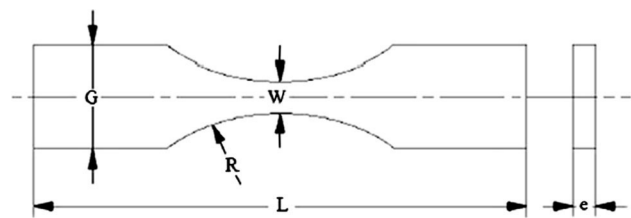


Fig. 1—Schematic representation of the fatigue specimens ( $e = 1.5 \text{ mm}$ ,  $G = 15 \text{ mm}$ ,  $L = 95 \text{ mm}$ ,  $R = 30 \text{ mm}$ , and  $W = 3.8 \text{ mm}$ ).

190 of tensile samples, load axis coincided with the rolling  
 191 direction. Tests were conducted under load control in a  
 192 resonant testing machine Rumul Mikroton, working at  
 193 frequencies around 150 Hz. The imposed stress ratio  
 194 ( $R = \sigma_{\min}/\sigma_{\max}$ ) was 0.1. Before tests, samples were  
 195 grinded and polished at the sides and corners up to the  
 196 same roughness of the sheet surface  
 197 ( $R_a = 0.18 \pm 0.02 \mu\text{m}$ ) in order to avoid premature  
 198 fracture due to laser cutting defects as demonstrated by  
 199 the authors in a previous study.<sup>[27]</sup> It was shown that  
 200 laser beam produces a significant increase of edge  
 201 roughness due to overlapping of molten steel which  
 202 causes a strong reduction of fatigue limit. On the other  
 203 hand, microstructural changes due to laser heat were not  
 204 discerned.

### 205 III. RESULTS AND DISCUSSION

#### 206 A. Microstructural Analysis

207 Figure 2 shows the X-ray diffraction patterns of the  
 208 studied samples. It can be seen that no peaks related to  
 209  $\epsilon$ -martensite were detected even for the minor reduction.  
 210 The fact that  $\epsilon$ -martensite consists of overlapping  
 211 stacking faults<sup>[17,28]</sup> implies very low intensities so that  
 212 it was not identified by this technique. On the other  
 213 hand, at increasing cold rolling reduction, austenite  
 214 peaks gradually decreased due to the transformation to  
 215  $\alpha'$ -martensite, whose volume fraction is given in Table I.  
 216 It has to be mentioned that martensite volume content  
 217 may differ depending on the technique used,<sup>[29,30]</sup> in the  
 218 case of X-ray diffraction, measurements are affected by  
 219 texture.

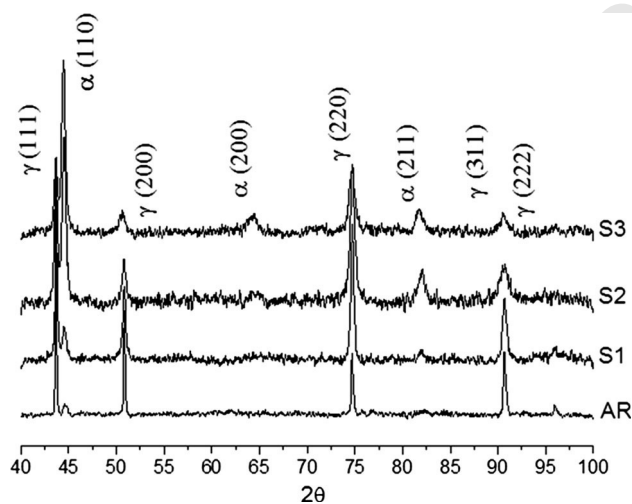


Fig. 2—X-ray diffraction patterns of the studied samples.

Stacking fault energy (SFE) plays a very important  
 role in the deformation mechanisms. In general, a lower  
 SFE makes dislocation cross-slip more difficult, result-  
 ing in less dislocation mobility and promoting marten-  
 sitic phase transformation. Using the equation suggested  
 by Schramm and Reed<sup>[31]</sup> (Eq. [2]), the SFE of this steel  
 results equal to 11.2 mJ/m<sup>2</sup>. SFE values for the most  
 common austenitic stainless steels series AISI 300<sup>[32]</sup> are  
 in the range from 9.2 to 80.3. Therefore, the studied  
 301LN displays a low value, and as a consequence  
 deformation of induced martensite increases signifi-  
 cantly with cold rolling reduction.

$$\text{SFE (mJ/m}^2\text{)} = -53 + 6.2(\text{pctNi}) + 0.7(\text{pctCr}) + 3.2(\text{pctMn}) + 9.3(\text{pctMo}) \quad [2]$$

The microstructure of the AR condition shows  
 equiaxial austenitic grains (average grain size of  
 $11.7 \pm 4.1 \mu\text{m}$ ) randomly oriented with twins created  
 during annealing treatment (Figure 3). For cold-rolled  
 samples, progressive formation of slip bands can be  
 observed in addition to martensitic transformation  
 (Figure 4).  $\alpha'$ -martensite nucleates mainly at shear  
 bands intersections and grain boundaries for S1 sam-  
 ples, even though it extends rapidly across the entire  
 grain at increasing cold rolling reductions (S2 and S3),  
 Figure 5. There was no evidence of the presence of  
 $\epsilon$ -martensite even for the minor cold rolling reduction.  
 It has to be considered that the analyzed microstructures  
 were not completely resolved by EBSD. As it is well  
 known, highly deformed grains cannot be reliably  
 indexed using this technique as Roa *et al.*<sup>[33]</sup> observed  
 for TWIP steels, and in some areas it was not possible to  
 distinguish between slip bands in austenite and  
 martensite.

After reversion treatments no peaks of  $\alpha'$ -martensite  
 were detected, even for the samples coming from the  
 steel condition with the highest percentage of this phase,  
*i.e.*, RS3. Microstructural characteristics after reversion  
 depend on the prior percentage of cold rolling reduction.

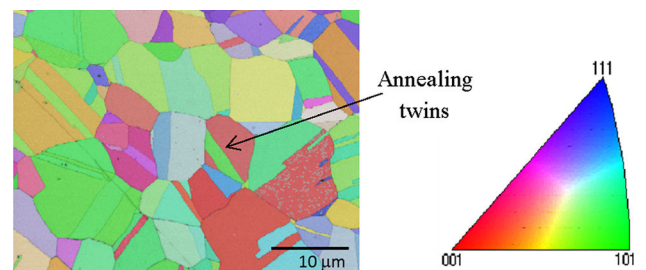


Fig. 3—EBSD orientation map of annealed sample (AR).

Table I. Volume Fraction of Strain-Induced Martensite as a Function of Cold Rolling Reduction

	AR	S1	S2	S3
Cold rolling Reduction (pct)	0	10	20	40
Volume fraction of martensite (pct)	0	$9 \pm 3$	$28 \pm 7$	$38 \pm 5$

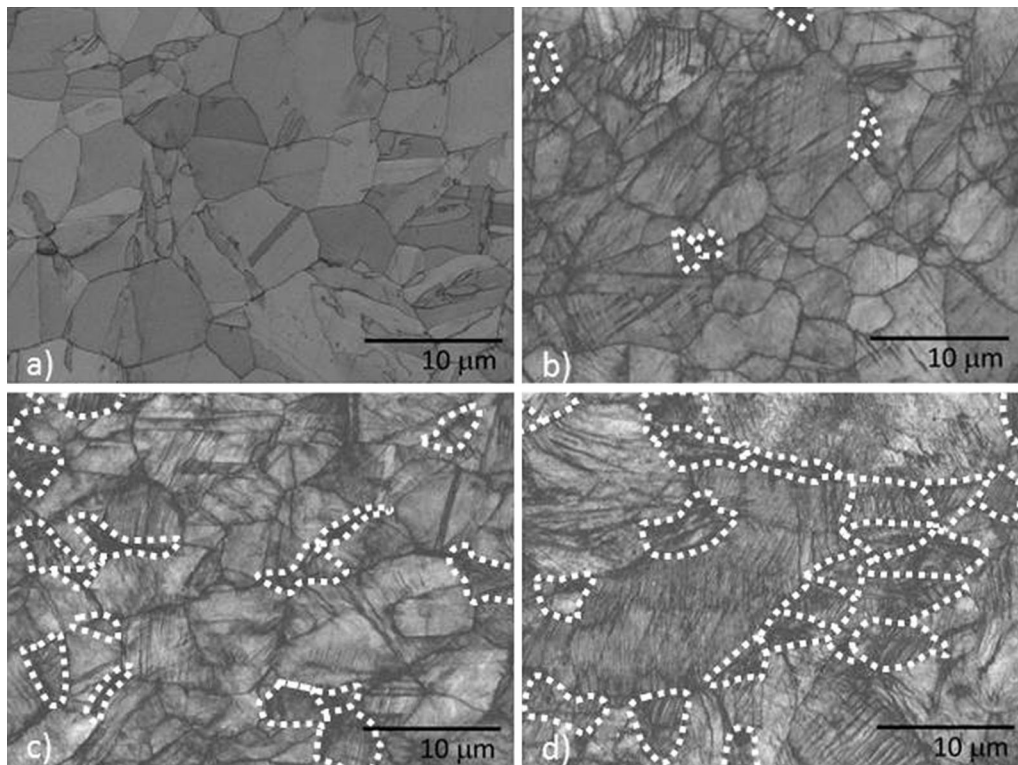


Fig. 4—Microstructure of the studied steel in annealed condition (a) and after cold rolling reductions of: (b) 10 pct, (c) 30 pct, and (d) 40 pct. Martensite phase identification by EBSD is enclosed in white dotted lines.

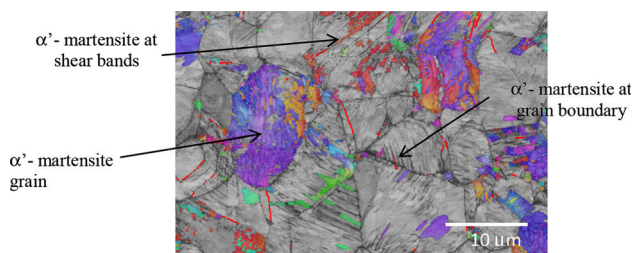


Fig. 5—EBSD orientation map of 20 pct cold-rolled sample (S2).

Small amounts of pre-existing martensite ( $9 \pm 3$  pct), led to a slight reduction on the average grain size, up to  $8.8 \pm 2.9 \mu\text{m}$ , compared to  $3.8 \pm 1.9$  and  $2.3 \pm 1.5 \mu\text{m}$  achieved for martensite contents of 28 and 38 pct, respectively. In this regard, conventional industrial cold rolling process does not allow reducing grain size such as severe cold rolling and advanced thermo-mechanical process, where microstructure becomes ultrafine-grained ( $<100 \text{ nm}$ ) and even nanocrystallined ( $<50 \text{ nm}$ ).<sup>[8,10,13–15,17]</sup>

The wide grain size distribution observed for samples RS2 and RS3 (Figure 6) points out that austenite recrystallization takes place in various types of nucleation sites, as demonstrated by Rajasekhara *et al.*<sup>[10]</sup> This feature is typical of diffusion-type reversion mechanisms, in contrast with shear-type reversion mechanism where nucleation is time-independent and no austenite grain growth is observed.

## B. Monotonic Mechanical Properties

It is well known that mechanically induced martensite can enhance mechanical properties.<sup>[34–39]</sup> As demonstrated by the data in Figure 7, the higher the percentage of martensite, the higher the values of yield stress, ultimate strength, and hardness. It is important to point out that even for low amounts of pre-existing martensite, a relevant yield stress increase was observed. This becomes clear when yield stress values of AR and S1 samples are compared, the presence of 9 pct of pre-existing martensite leads to an increase from 360 to 650 MPa. On the other hand, the gap between yield stress and ultimate tensile strength becomes narrower as the cold rolling reduction rises, *i.e.*, the as-received steel condition displayed a ratio of 0.42 which increased up to 0.97 at cold reduction of 40 pct.

Significant discrepancy still exists in explaining the strengthening mechanisms of metastable austenitic stainless steels and, in concrete, the effect of the strain-induced  $\alpha'$ -martensite phase. Since the highly dislocated  $\alpha'$ -phase is much harder than the austenite, some authors<sup>[40,41]</sup> consider austenite-martensite mixtures as composites of soft austenitic matrix with hard martensite dispersion. Spencer *et al.*<sup>[42]</sup> demonstrated that martensite sustains a clearly higher stress than austenite, concluding that  $\alpha'$ -martensite acts as the reinforcing phase. In that sense, studies developed by Narutani *et al.*<sup>[43]</sup> for an AISI 301 steel concluded that for high martensite contents ( $>20$  pct), the strengthening was



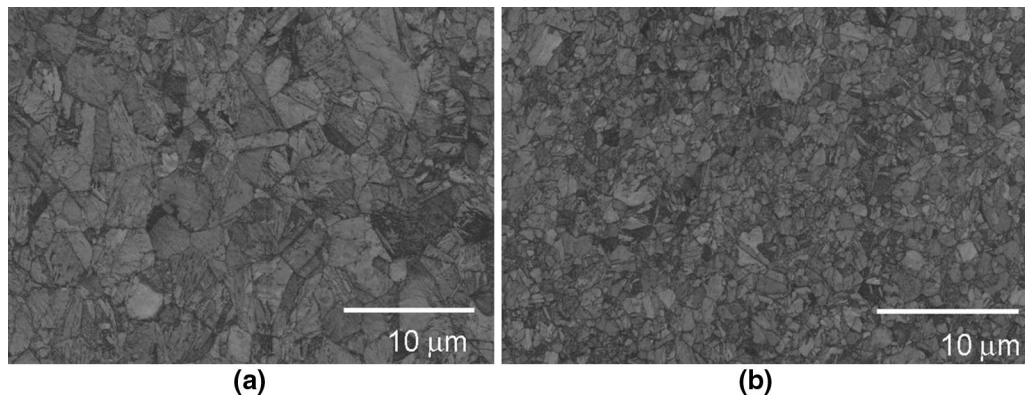


Fig. 6—Microstructure of (a) RS2 and (b) RS3 samples.

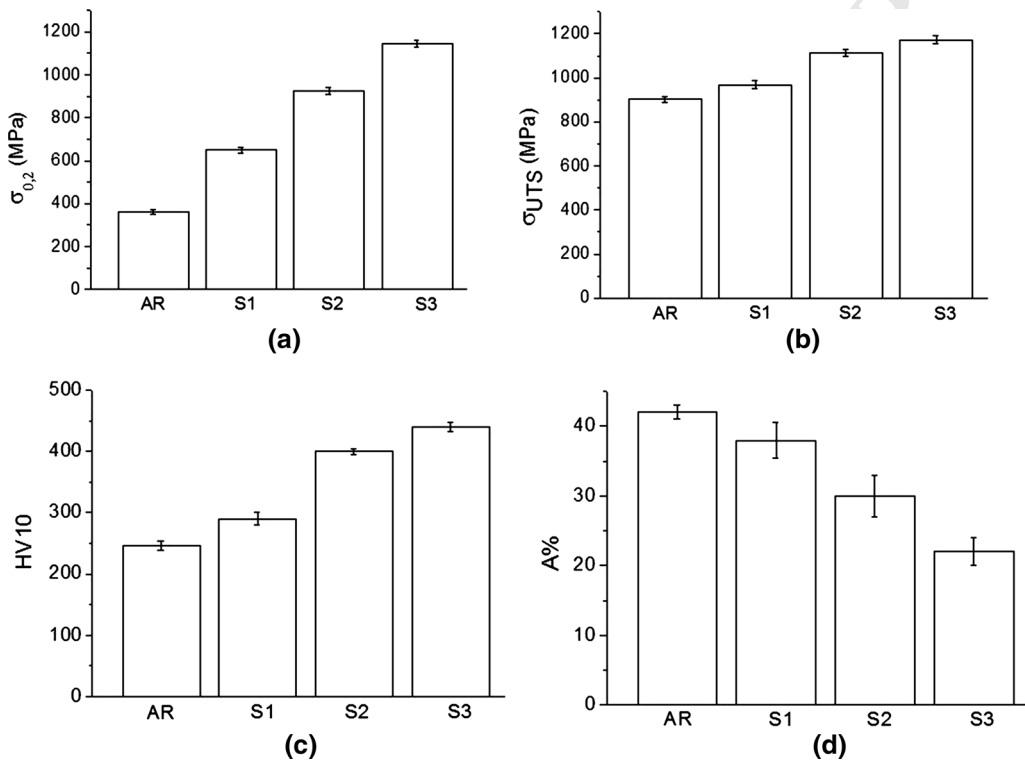


Fig. 7—Mechanical properties of steel after cold rolling: (a) yield strength, (b) ultimate strength, (c) hardness, and (d) ductility.

305 related to the hardening effect of the martensite by itself,  
 306 while below this content, the formation of  $\alpha'$ -martensite  
 307 strengthens the steel by accelerating the dislocation  
 308 generation in austenite. This effect was attributed to  
 309 the accommodation of the volume expansion related to  
 310 the transformation. Moreover, not only the influence of  
 311  $\alpha'$ -martensite, but also the austenite strengthening, plays  
 312 an important role on mechanical properties. As shown in  
 313 Figure 8, nanoindentation measurements performed on  
 314 austenitic grains revealed the effect of strain-hardening  
 315 as increasing cold rolling reduction. The average hard-  
 316 ness value displayed for the annealed condition (AR) was  
 317 almost 50 pct lower than for cold-rolled sample S3.

318 Combined contribution of rising martensite transfor-  
 319 mation and austenite hardening causes a reduction of  
 320 plastic deformation. As it can be observed in  
 321 Figure 7(d), the ductility is inversely proportional to  
 322 the initial amount of martensite. Numerous studies have  
 323 focused on understanding the TRIP effect. The most  
 324 widely accepted interpretation<sup>[44–47]</sup> is that not only the  
 325 total amount of induced martensite is significant, but  
 326 also the rate of transformation for a given plastic strain  
 327 and at which point it takes place, are the factors that  
 328 govern the ductility. The evolution of martensite trans-  
 329 formation shown in Figure 9 demonstrates the validity  
 330 of this interpretation. In this sense, for sample S2, whose  
 331

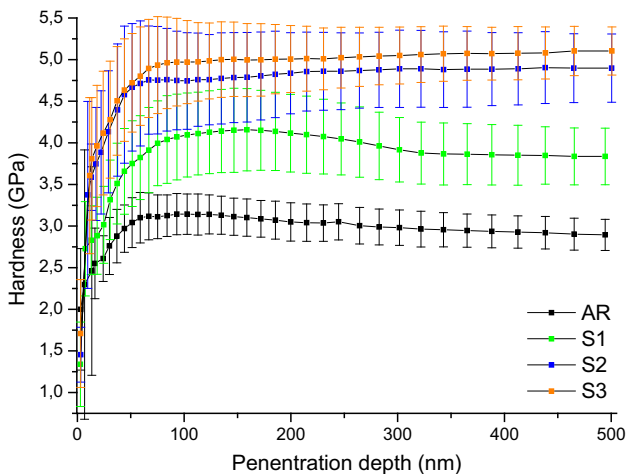


Fig. 8—Austenite hardness of the annealed (AR) and cold-rolled (S1, S2, S3) steel.

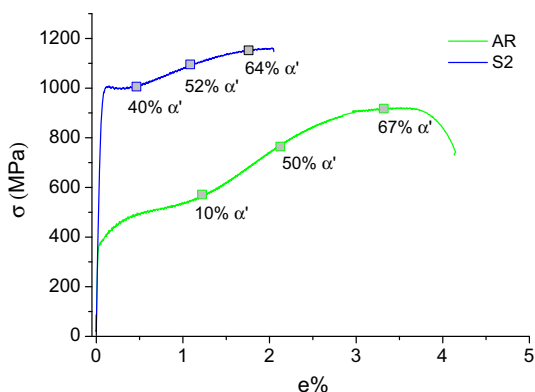


Fig. 9—Stress–strain curves for AR and S3 steel conditions indicating the percentage of  $\alpha'$ -martensite at 30, 60, and 90 pct of their respective total elongation values.

initial martensite content was 28 pct, transformation occurs rapidly in comparison with AR, resulting in abrupt work hardening and, consequently, premature fracture.

Significant differences can be observed concerning fracture surfaces of tensile tested specimens. AR showed high density of dimples, generally associated with high plastic strain typical of ductile fracture (Figure 10(a)). For increasing pre-existing  $\alpha'$ -martensite, fracture aspect is progressively shifting towards brittle (Figure 10(b) to (d)), with faceted areas and microcracks clearly distinguished. Assuming that the inclusions volume fraction is constant and at a very low level, the main embrittlement mechanisms are expected to be decohesion at the austenite-martensite interface or separation of adjacent islands and localized deformation of martensite.

Figure 11 shows the effect of reversion treatments on the mechanical properties. It is important to point out that even small amount of pre-existing martensite (RS1) influences mechanical properties in such a way that yield strength achieves values higher than 40 pct comparing with untreated samples (AR) and with similar ductility.

In this sense, it is clear that the smaller the grain size (corresponding to the steel conditions with high percentage of pre-existing martensite, RS2 and RS3) the higher the strength and the hardness. However, the ductility of the RS3 condition still displays at least 50 pct less ductility than AR samples. Detailed analysis of fracture surfaces reveals that, although RS3 presented large number of small dimples compared to AR (Figure 12), which it is known to increase ductility, microcracks and cracks randomly distributed on surface fracture were identified (Figure 13). These microcracks were also observed in cold-rolled samples S3. In this regard, it was assumed that contents of pre-existing martensite from cold rolling were still present in RS3 samples, *i.e.*, incomplete  $\alpha' \rightarrow \gamma$  transformation phase took place during reversion treatments. Thus, for samples cold rolled at 40 pct thickness reduction (S3), it is necessary to apply higher temperatures or extend holding time to achieve fully austenitic microstructure.

It is well known that yield stress and hardness of a metallic material increase with decreasing grain size. In particular, the empirical Hall–Petch equation has been found to express this grain-size dependence.<sup>[48,49]</sup> Figure 14 clearly shows this inverse relationship, *i.e.*, both yield strength and hardness increase linearly when  $d^{-1/2}$  goes from 11.7  $\mu\text{m}$ , corresponding to the untreated steel (AR), up to 2.3  $\mu\text{m}$ , value achieved after reversion treatments (RS3). These results are consistent and complement those shown by Huang *et al.*<sup>[28]</sup> which demonstrated that the Hall-Petch relationship for AISI 301LN held well down to 0.74  $\mu\text{m}$  of mean austenitic grain size, while measurements on AISI 301 displayed deviation at about 3  $\mu\text{m}$  grain size.<sup>[6]</sup>

### C. Fatigue Tests

Studies on the fatigue response of metastable stainless steels report different behaviors depending on the testing conditions.<sup>[50–54]</sup> The formation of martensite during deformation is known to be harmful in the low cycle fatigue regime, *i.e.*, under strain-control, while a small amount of martensite can be beneficial in the HCF regime.

A previous paper presented by the authors<sup>[55]</sup> demonstrated the possibility of improving the fatigue life of a metastable austenitic stainless steel by inducing martensitic transformation via torsion deformation previously to the HCF tests. In the present study, a similar trend was observed for cold-rolled samples S2 and S3. As shown in Table II, fatigue limits corresponding to those steel conditions are significantly higher in comparison with fully austenite microstructure (AR). After fatigue tests, X-ray diffraction patterns (Figure 15) revealed that  $\alpha'$ -martensite increased up to 44 pct when the initial microstructure is fully austenitic (AR), while the amount created for the steel condition with a 28 pct of pre-existing martensite (S2) grew up 50 pct. As a result, significant differences were found regarding surface roughness associated with  $\gamma \rightarrow \alpha'$  transformation, *i.e.*,  $0.325 \pm 0.018 \mu\text{m}$  and  $0.198 \pm 0.021 \mu\text{m}$  for AR and S2, respectively, compared with values lower than 0.1  $\mu\text{m}$  before fatigue tests. These results are in

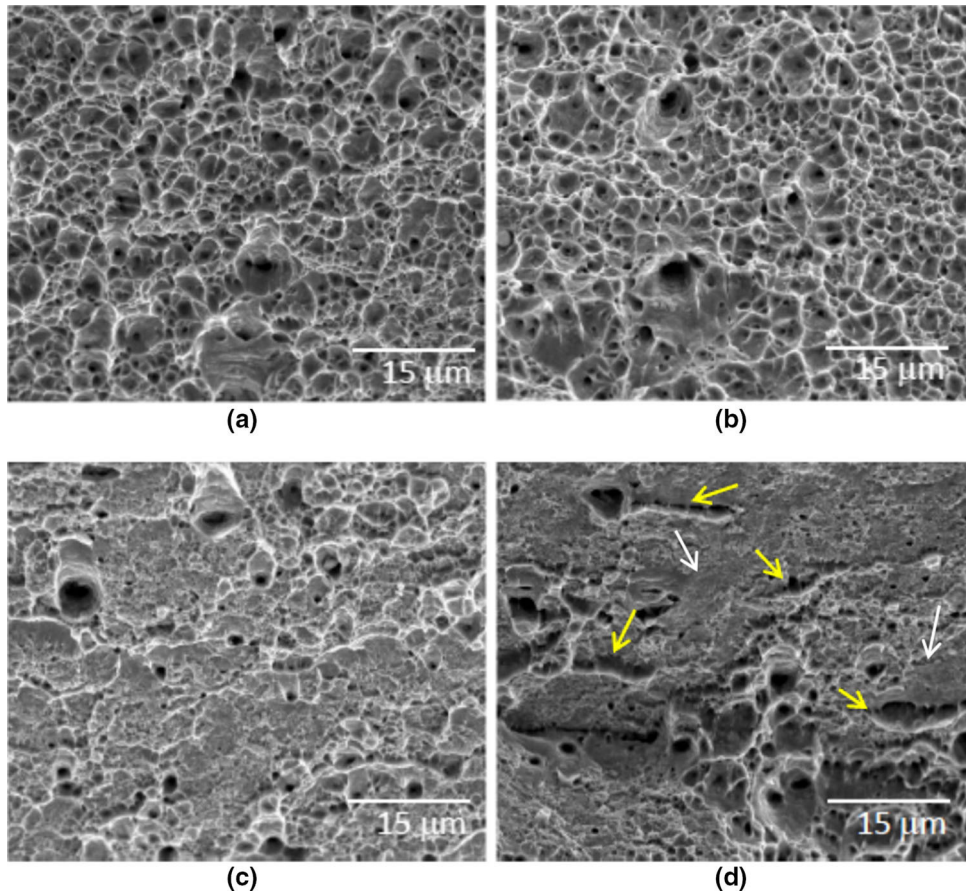


Fig. 10—SEM images of the fracture surfaces of tensile samples of: (a) AR, (b) S1, (c) S2, and (d) S3, yellow arrows indicate the presence of microcracks and white arrows point to faceted areas.

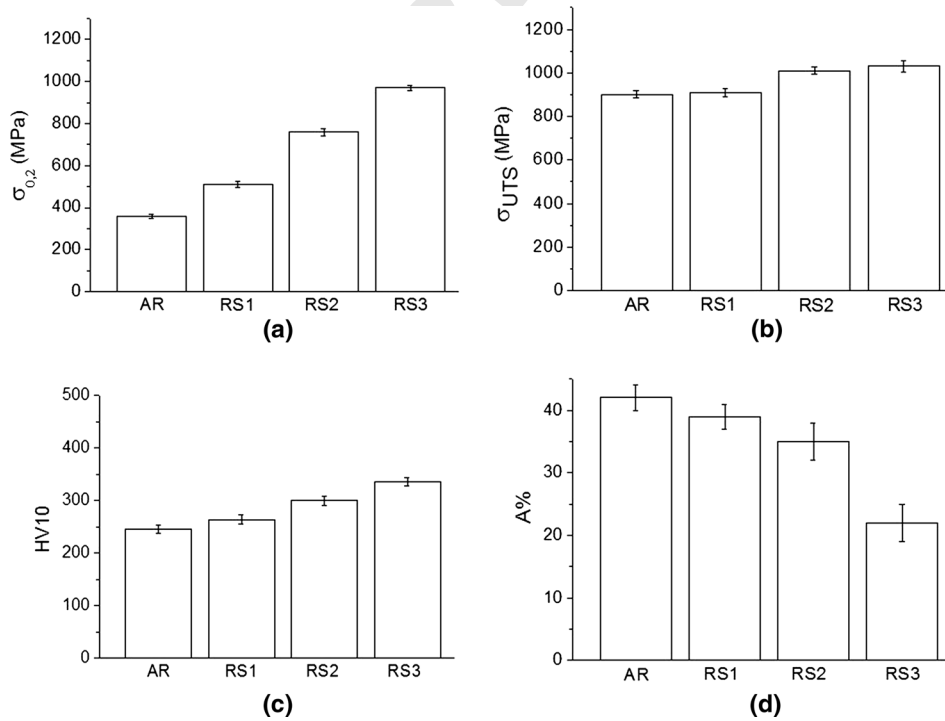


Fig. 11—Mechanical properties of steel after reversion: (a) yield strength, (b) ultimate strength, (c) hardness, and (d) ductility.

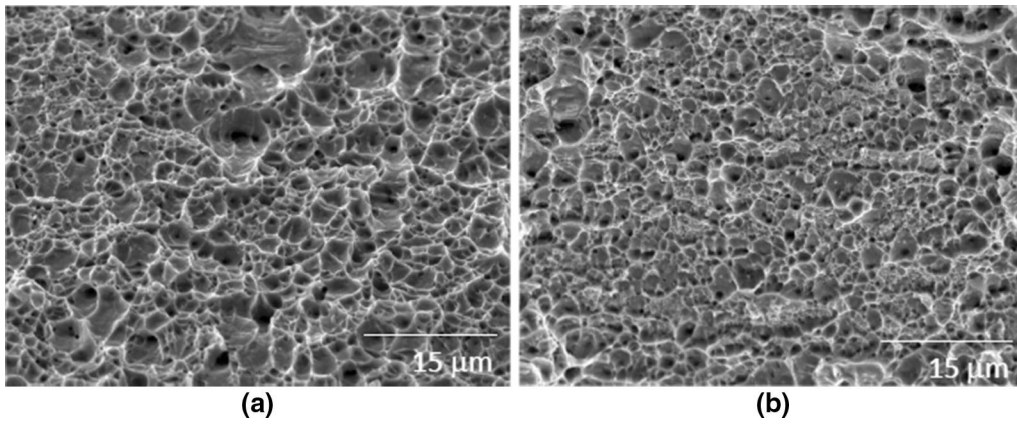


Fig. 12—SEM images of the fracture surfaces of tensile samples corresponding to: (a) Annealed steel, and (b) Reverted condition (RS3).

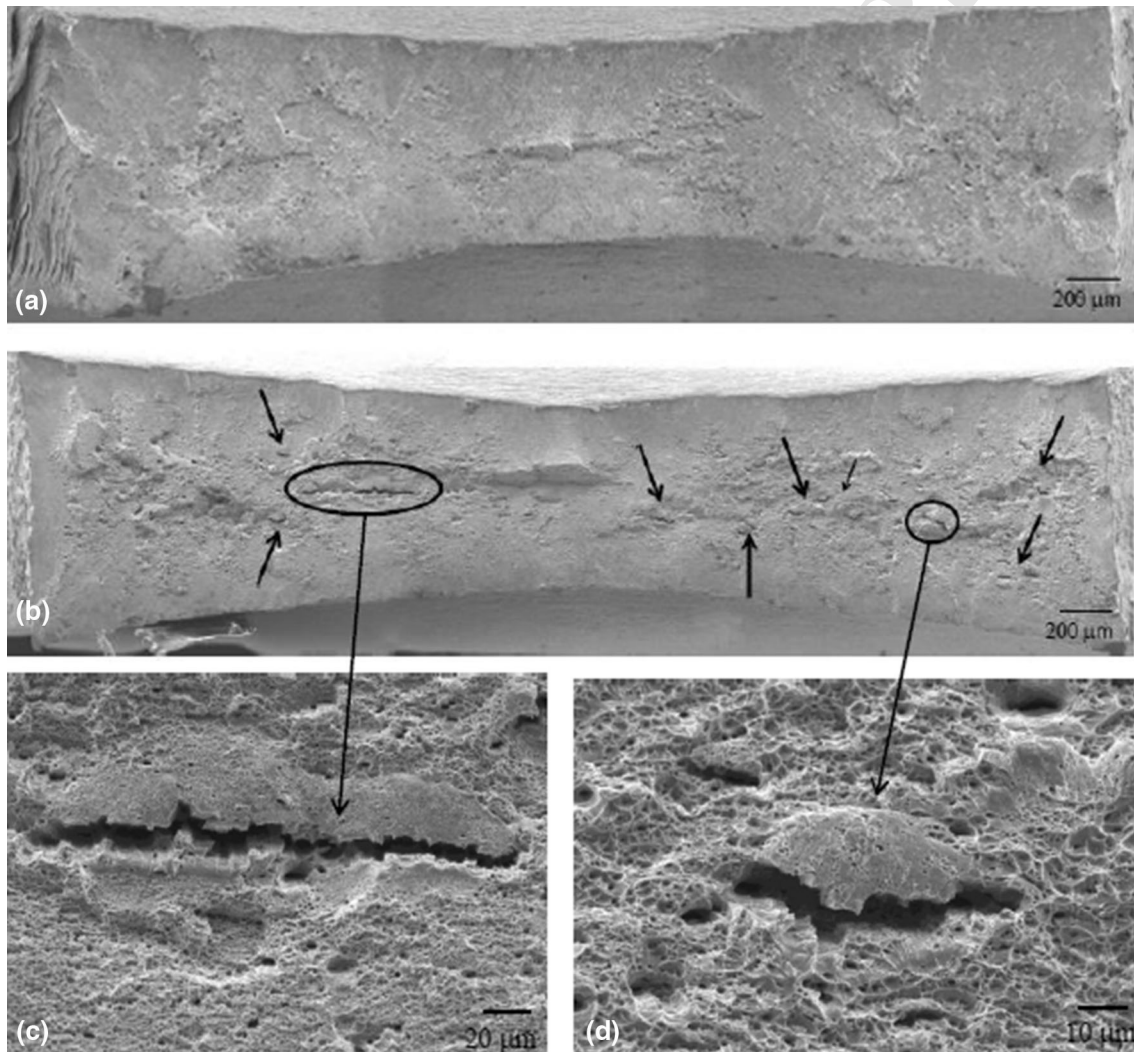


Fig. 13—SEM images of the fracture surfaces of tensile samples of: (a) Annealed steel (AR), and (b) Reverted condition (RS3), (c, d) Magnifications of cracks observed in figure b.

413 agreement with several studies which have pointed out  
 414 that volume expansion associated with the martensitic  
 415 transformation lead to the components distortion,  
 416 dimensional changes, and even failure under extreme  
 417 working conditions.<sup>[56,57]</sup> Moreover, authors demon-  
 418 strated in a previous study carried out on the same steel  
 419 grade,<sup>[58]</sup> that the amount of martensite formed during  
 420 the first cycles of fatigue tests remains almost stable and  
 421 martensite plates grow in height but neither in width nor  
 422 in length. In this sense, it is assumed that higher  
 423 roughness induces fatigue nucleation sites which dra-  
 424 matically influence fatigue behavior. In this regard, AR  
 425 samples display higher “fatigue sensitivity” compared to  
 426 S2 and S3. This parameter introduced by Fleck *et al.*,<sup>[59]</sup>  
 427 is defined as the ratio between the maximum stress that

the specimen is able to reach after  $10^6$  cycles without fail  
 and the ultimate tensile strength  $[1 - (\sigma_{max}/\sigma_{UTS})]$ .  
 Fatigue sensitivity ranges from 0 to 1, so values closer  
 to 0 indicate less sensitivity to fatigue. In that sense,  
 results shown that at increasing percentage of pre-exist-  
 ing martensite, *i.e.*, S1 to S3, fatigue sensitivity progres-  
 sively decreases becoming half of the value displayed for  
 the fully austenitic steel (AR).

Grain size refinement achieved by reversion treat-  
 ments led to fatigue limits clearly higher than the value  
 corresponding to AR condition, Table III. This effect  
 was more pronounced for samples RS2 and RS3, but  
 even for the steel condition with the lowest percentage of  
 pre-existing  $\alpha'$ -martensite (RS1) an increase of 12 pct on  
 fatigue limit was measured. This is consistent and

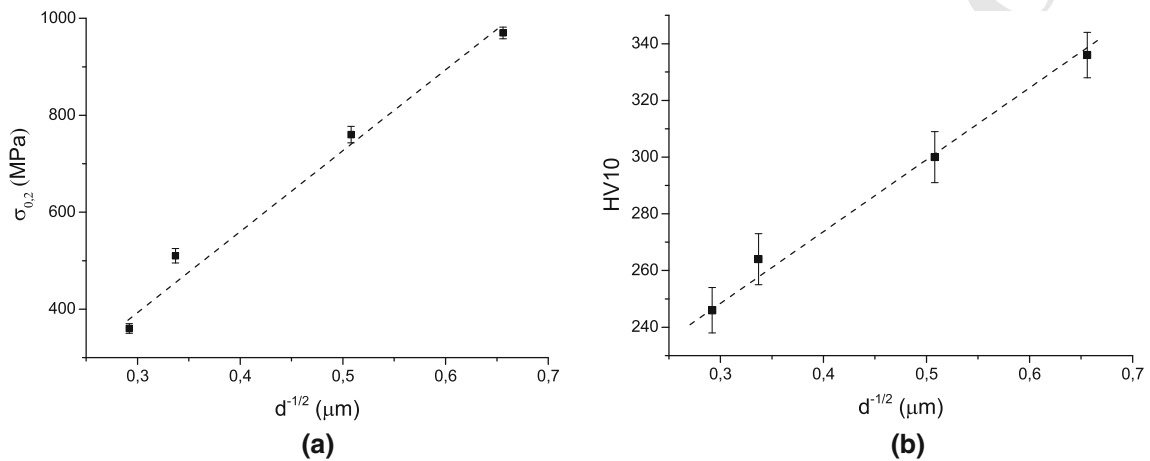


Fig. 14—Dependence of the grain size on: (a) yield strength and (b) hardness.

**Table II. Fatigue Limit and Fatigue Sensitivity for Studied Steel Conditions**

Steel Conditions	AR	S1	S2	S3
$\sigma_{max}$ (MPa)	$570 \pm 56$	$680 \pm 49$	$895 \pm 71$	$956 \pm 88$
Fatigue sensitivity	0.37	0.30	0.20	0.18

**Table III. Fatigue Limit and Fatigue Sensitivity After Reversion Treatments**

Steel Conditions	AR	RS1	RS2	RS3
$\sigma_{max}$ (MPa)	$570 \pm 56$	$640 \pm 44$	$795 \pm 58$	$880 \pm 43$
$1 - (\sigma_{max}/\sigma_{UTS})$	0.37	0.30	0.22	0.15

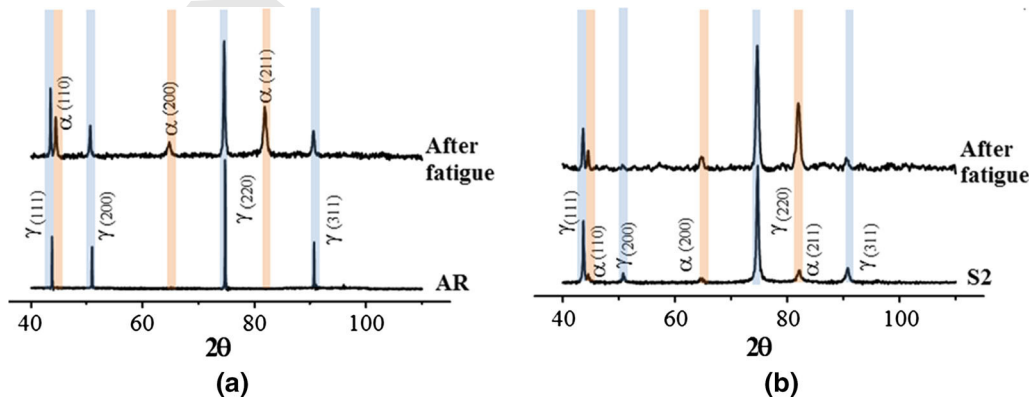


Fig. 15—X-ray diffraction patterns of the annealed (AR) and cold-rolled (S2) samples after  $10^6$  fatigue cycles.

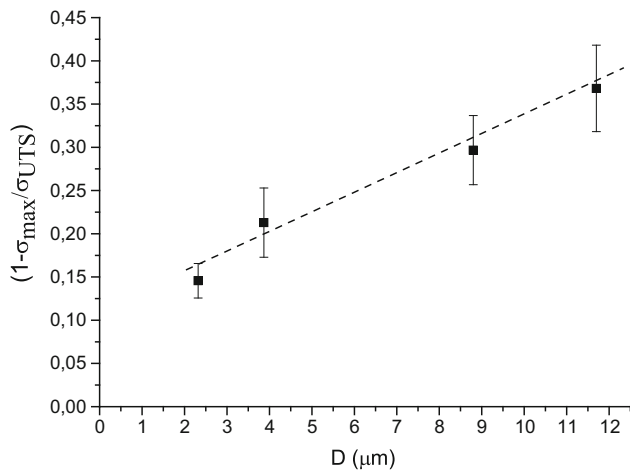


Fig. 16—Effect of grain size on fatigue sensitivity.

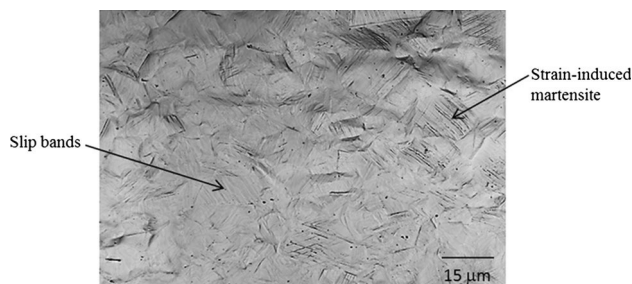


Fig. 17—Slip bands and strain-induced martensite after fatigue tests on annealed steel (AR).

443 complements earlier investigations<sup>[16,60]</sup> carried on  
 444 reverted AISI 301LN steel with higher percentages of  
 445 pre-existing  $\alpha'$ -martensite (>80 pct) than those studied  
 446 in this work. It was also observed that  $\gamma \rightarrow \alpha'$  phase  
 447 transformation was significantly reduced at decreasing  
 448 grain size. After fatigue tests, the amount of strain-in-  
 449 duced martensite was close to 44 pct for the AR, while  
 450 reverted samples (RS3) showed values not higher than  
 451 23 pct. As some authors have demonstrated,<sup>[61–63]</sup> basi-  
 452 cally two reasons can explain this behavior: the higher  
 453 strength of fine-grained austenite which slows up the  
 454 strain-induced martensite formation and the increasing  
 455 of SFE due to grain refinement, taking into account that  
 456 higher SFE means higher austenite stability.

457 Another important feature achieved by reverted  
 458 austenite microstructure is the progressive reduction of  
 459 fatigue sensitivity as grain size decreases (Figure 16).  
 460 SEM analysis performed in plain view areas close to the  
 461 fracture surface revealed the formation of intensive slip  
 462 bands crossing the grains for the condition with bigger  
 463 grain size (AR), Figure 17, compared to RS3 samples  
 464 where less density of slip bands was observed. This trait,  
 465 even observed for ultrafine-grained and nanocrystalline  
 466 microstructures,<sup>[15,16]</sup> together with lower fatigue-in-  
 467 duced martensite content at the samples surface and  
 468 its corresponding volume expansion (as much as  
 469 4 pct)<sup>[64–66]</sup> was assumed to be critical to reduce crack  
 470 nucleation sites and as a consequence fatigue sensitivity.

#### IV. CONCLUSIONS

The effect on microstructural characteristics and  
 mechanical properties, both monotonic and cyclic, of  
 the martensite induced by industrial cold rolling pro-  
 cesses, with a thickness reduction up to 40 pct, was  
 analyzed. Moreover, the influence of reversion heat  
 treatments, that remove martensite and lead to a smaller  
 austenitic grain size, was studied too. The following  
 conclusions can be extracted concerning the influence of  
 strain-induced martensite:

- No evidence of  $\epsilon$ -martensite was detected on the  
 studied cold-rolled samples. The formation of  
 $\alpha'$ -martensite develops mainly at shear bands and  
 increases progressively with the cold rolling reduc-  
 tion, but not linearly.
- Small amounts of  $\alpha'$ -martensite, formed after 10 pct  
 of cold rolling, increase more than 50 pct the yield  
 stress, as compared with AR, whereas after 40 pct of  
 cold working yield stress triplicates the initial one.
- Cold rolling has a positive effect on the fatigue limit  
 too.  $\alpha'$ -martensite formed by 10-pct cold rolling  
 enhanced fatigue limit around 20 pct compared to  
 AR. Higher cold working levels allowed values 60 pct  
 higher.

With regard to the effect of reversion treatments, it  
 can be stated that:

- Reversion treatments demonstrated to be a feasible  
 way to obtain grain refinement, simultaneously  
 avoiding the presence of martensite. The average  
 austenitic grain size decreased by 25 pct for samples  
 with 10 pct of cold working reduction, whereas  
 80 pct of grain refinement was reached after 40 pct  
 of cold rolling.
- Hall-Petch relationship between austenite grain size,  
 yield strength, and hardness works well for reversed  
 microstructures ranging from 0.29 to 0.66  $\mu\text{m}$ .
- Even for small amounts (less than 10 pct) of pre-ex-  
 isting martensite reversion treatments provided a  
 significant increment (40 pct) on yield stress over the  
 AR.
- Upon reversion, enhanced fatigue limit, as compared  
 to AR, was measured for specimens previously  
 subjected to 20 pct and 40 pct of cold rolling  
 reduction. On the other hand, less intensively rolled  
 samples (only 10 pct of reduction) did not display a  
 higher fatigue limit.

#### ACKNOWLEDGMENTS

The present work was carried out within the scope  
 of MAT09-14461 project, supported by the Spanish  
 Ministry of Economy. We are grateful to “*Direcció  
 General de Recerca del Comissionat per a Universitats i  
 Recerca de la Generalitat de Catalunya*” for recogniz-  
 ing CIEFMA as a consolidated Research Group  
 (2009SGR). Dr. J. J. Roa would like to thank Juan de

REFERENCES

1. F. Placidi and F. Frascchetti: *Potential application of stainless steel for vehicle crashworthiness structures*. Technical report, Cenro sviluppo materiali, Italy.
2. A. Di Schino, J.M. Kenny, M.G. Mecozzi, and M. Barteri: *J. Mater. Sci.*, 2000, vol. 35, pp. 4803–08.
3. T. Christiansen and M.A.J. Somers: *Metal. Mater. Trans. A*, 2006, vol. 37A, pp. 675–82.
4. S.S. Hecker, M.G. Stout, and J.L. Smith: *Metall. Trans.*, 1982, vol. 13A, pp. 619–26.
5. H.F.G. de Abreu, M.J.G. da Silva, L.F.G. Herculano, and H. Bhadeshia: *Mater. Res.*, 2009, vol. 12, pp. 291–97.
6. A. Di Schino, M. Barteri, and J.M. Kenny: *J. Mater. Sci. Lett.*, 2002, vol. 21, pp. 751–53.
7. J.Y. Choi and W. Jin: *Scr. Mater.*, 1997, vol. 36, pp. 99–104.
8. M. Karimi, A. Najafzadeh, A. Kermanpur, and M. Eskandari: *Mater. Charact.*, 2009, vol. 60, pp. 1220–23.
9. M.C. Somani, L.P. Karjalainen, A. Kyröläinen, and T. Taulavuori: *Mater. Sci. Forum*, 2007, vols. 539–543, pp. 4875–7880.
10. S. Rajasekhara, L.P. Karjalainen, A. Kyröläinen, and P.J. Ferreira: *Mater. Sci. Eng. A*, 2010, vol. 527, pp. 1986–96.
11. A. Di Schino and J.M. Kenny: *Mater. Lett.*, 2003, vol. 57, pp. 3182–85.
12. A.S. Hamada, L.P. Karjalainen, and M.C. Somani: *Mater. Sci. Eng. A*, 2006, vol. 431, pp. 211–17.
13. R.D.K. Misra, B. Ravi Kumar, M. Somani, and P. Karjalainen: *Scr. Mater.*, 2008, vol. 59, pp. 79–82.
14. M.C. Somani, P. Juntunen, L.P. Karjalainen, R.D.K. Misra, and A. Kyröläinen: *Metall. Mater. Trans. A*, 2009, vol. 40A, pp. 729–44.
15. A.S. Hamada, L.P. Karjalainen, P.K.C. Venkata v, and R.D.K. Misra: *Mater. Sci. Eng. A*, 2011, vol. 528, pp. 3890–96.
16. A. Järvenpää, L. Pentti Karjalainen, and M. Jaskari: *Int. J. Fatigue*, 2013, vol. 65, pp. 93–98.
17. J. Huang, X. Ye, J. Gu, X. Chen, and Z. Xu: *Mater. Sci. Eng. A*, 2012, vol. 532, pp. 190–95.
18. O.V. Mishin, D.J. Jensen, and N. Hansen: *Mater. Sci. Eng. A*, 2003, vol. 342, pp. 320–28.
19. T.S. Wang, J.G. Peng, Y.W. Gao, F.C. Zhang, and T.F. Jing: *Mater. Sci. Eng. A*, 2005, vol. 407, pp. 84–88.
20. A. Mateo, A. Hernández, A. Zapata, P. Rodríguez-Calvillo, G. Fargas, J. Calvo, and D. Casellas: *XII Congreso Iberoamericano de Materiales IBEROMAT XII*, Univ. Alicante A-20, 2012.
21. ASTM E975-03: *Standard Practice for X-Ray Determination of Retained Austenite in Steel with Near Random Crystallographic Orientation*, ASTM International, West Conshohocken, 2003.
22. W.C. Oliver and G.M. Pharr: *J. Mater. Res.*, 1992, vol. 7, pp. 1564–83.
23. W.C. Oliver and G.M. Pharr: *J. Mater. Res.*, 2004, vol. 19, pp. 3–20.
24. ASTM E 8-04: *Standard Test Methods for Tension Testing of Metallic Materials*, 2008.
25. A.M. Mood and W.J. Dixon: *J. Am. Stat. Assoc.*, 1948, vol. 43 (241), pp. 109–126.
26. D. Grove and F. Campean: *Test*, 2008, vol. 24, pp. 485–97.
27. A. Mateo, G. Fargas, J.J. Roa, and J. Calvo: *Mater. Test.*, 2015, vol. 57, pp. 2–5.
28. J.X. Huang, X.N. Ye, and Z. Xu: *J. Iron Steel Res. Int.*, 2012, vol. 19 (10), pp. 59–63.
29. J. Talonen, P. Aspengren, and H. Hänninen: *Mater. Sci. Technol.*, 2004, vol. 20 (12), pp. 1506–512.
30. A.M. Beese and D. Mohr: *Exp. Mech.*, 2011, vol. 51, pp. 667–76.
31. R.E. Schramm and R.P. Reed: *Metall. Trans.*, 1975, vol. 6A, pp. 1345–51.
32. A.F. Padilha, R.L. Plaut, and P.R. Rios: *ISIJ Int.*, 2003, vol. 43 (2), pp. 135–43.
33. J.J. Roa, G. Fargas, J. Calvo, E. Jiménez-Piqué, and A. Mateo: *Mater. Sci. Eng. A*, 2015, vol. 628, pp. 410–18.
34. F. Lécroisey and A. Pineau: *Metall. Trans.*, 1972, vol. 3, pp. 387–96.
35. G.D. Huang, D.K. Matlock, and G. Krauss: *Metall. Trans. A*, 1989, vol. 20 (7), pp. 1239–46.
36. X.F. Fang and W. Dahl: *Mater. Sci. Eng. A*, 1991, vol. 141 (2), pp. 189–98.
37. T.S. Byun: *Acta Mater.*, 2003, vol. 51 (11), pp. 3063–3071.
38. J. Talonen, P. Nenonen, G. Pape, and H. Hanninen: *Met. Mater. Trans. A*, 2005, vol. 36 (2), pp. 421–32.
39. A.M. Beese and D. Mohr: *J. Mech. Phys. Solids*, 2012, vol. 60 (11), pp. 1922–40.
40. P.L. Mangonon and G. Thomas: *Metall. Trans.*, 1970, vol. 1 (6), pp. 1587–94.
41. I. Tamura: *Metal Sci.*, 1982, vol. 16 (5), pp. 245–53.
42. K. Spencer, J.D. Embury, K.T. Conlon, M. Véron, and Y. Bréchet: *Mater. Sci. Eng. A*, 2004, vols. 387–389, pp. 873–81.
43. T. Narutani: *Mater. Trans. JIM*, 1989, vol. 30 (1), pp. 33–45.
44. G.P. Sanderson and D.T. Llewellyn: *J. Iron Steel Inst.*, 1969, vol. 207 (8), pp. 1129–40.
45. A. Rosen, R. Jago, and T. Kjer: *J. Mater. Sci.*, 1972, vol. 7 (8), pp. 870–76.
46. N. Tsuchida and Y. Tomota: *Mater. Sci. Eng. A*, 2000, vol. 285 (1-2), pp. 345–52.
47. Y. Tomota, H. Tokuda, Y. Adachi, M. Wakita, N. Minakawa, A. Moriai, and Y. Morii: *Acta Mater.*, 2004, vol. 52 (20), pp. 5737–45.
48. J.N. Petch: *J. Iron Steel Inst.*, 1953, vol. 174, pp. 25–28.
49. E.O. Hall: *Proc. Phys. Soc.*, 1951, vol. 64B, pp. 747–53.
50. G.R. Chanani, S.D. Antolovich, and W.W. Gerberich: *Metall. Trans.*, 1972, vol. 3, pp. 2661–72.
51. G. Baudry and A. Pineau: *Mater. Sci. Eng.*, 1977, vol. 28, pp. 229–42.
52. C. Bathias and R.M. Pelloux: *Metall. Mater. Trans. B*, 1973, vol. 4B, pp. 1265–73.
53. J. Stolarz, N. Baffie, and T. Magnin: *Mater. Sci. Eng. A*, 2001, vols. 319–321, pp. 521–26.
54. M. Topic, R.B. Tait, and C. Allen: *Int. J. Fatigue*, 2007, vol. 29, pp. 656–65.
55. G. Fargas, A. Zapata, M. Anglada, and A. Mateo: *IOP Conf. Ser. Mater. Sci. Eng.*, 2009, vol. 5, p. 012008.
56. D. Mohan Lal, S. Renganarayanan, and A. Kalanidhi: *Cryogenics*, 2001, vol. 4, pp. 149–55.
57. D. Das, K.K. Ray, and A.K. Dutta: *Mater. Sci. Eng. A*, 2010, vol. 527, pp. 2182–93.
58. J.J. Roa, G. Fargas, E. Jiménez-Piqué, and A. Mateo: *Mater. Sci. And Eng. A*, 2014, vol. 597, pp. 232–36.
59. N.A. Fleck, K.J. Kang, and F. Ashby: *Acta Metall. Mater.*, 1994, vol. 42, pp. 365–81.
60. A.S. Hamada and L.P. Karjalainen: *Mater. Sci. Eng. A*, 2010, vol. 527, pp. 5715–22.
61. J.E. Jin, Y.S. Jung, and Y.K. Lee: *Mater. Sci. Eng. A*, 2007, vols. 449–451, pp. 786–89.
62. J.H. Jun and C.S. Choi: *Mater. Sci. Eng. A*, 1998, vol. 257, pp. 353–56.
63. R.D.K. Misra, Z. Zhang, Z. Jia, M.C. Somani, and L.P. Karjalainen: *Scr. Mater.*, 2010, vol. 63, pp. 1057–60.
64. Y.D. Wang, R.L. Peng, and R.L. McGreenyva: *Acta Mater.*, 2002, vol. 50, pp. 1717–34.
65. A. Bahadur, B.R. Kumar, and S.G. Chowdhury: *Mater. Sci. Technol.*, 2004, vol. 20, pp. 387–92.
66. T.V. Rajan, C.P. Sharma, and A. Sharma: *Heat treatment: Principles and Techniques*, 2 Eastern Economy Ednd ed., East West Academic Books LLC, Burlington, 2011, p. 200.